Monte Carlo Simulations of Cylinder-Forming ABC Triblock Terpolymer Thin Films

Peng Chen[†,‡] **and Haojun Liang***[,†,‡]

Hefei National Laboratory for Physical Sciences at Microscale, and Department of Polymer Science and Engineering, University of Science and Technology of China, Hefei, Anhui, 230026, People's Republic of China

Received: March 30, 2006; In Final Form: June 19, 2006

We systematically study the cylinder-forming ABC triblock terpolymer thin films using canonical ensemble Monte Carlo simulations. The simulated annealing procedure is applied to the self-assembling process. By judicious choice of the system dimensions, we elaborately investigate the effect of film thickness on the orientation of the cylinders. This confined triblock terpolymer system exhibits different phase behavior under the weak and strong surface fields. In addition, we also investigate the ensemble-averaged chain orientations and relative density profiles.

1. Introduction

Block copolymers are known to self-assemble into various ordered microstructures, having characteristic lengths which range from 10 to 100 nm[1] as may be determined by their molecular size. This property has attracted much interest in the area of photonic crystals, soft condensed matter physics, nanotechnology, etc.[2−4] Much effort has been paid to understand, predict, and control the structural formation of this macromolecular system.

Overall, the morphology of a block copolymer is determined mainly by the molecular architecture and the interaction of the different components comprising the copolymer.[5] Confinement effect, which is imposed by boundaries or interfaces, has a great influence on molecular conformation and assembly.[6−8] These may result either in the alignment of the bulk structure at the interface or the deviation of the microdomain structure from the bulk.[9,10] However, by tuning the confinement geometry and surface−polymers interactions, one can achieve molecular-level process control in self-assembling polymers and produce useful architectures.[11−16]

Many studies are centered on the control of morphology of block copolymer systems under various confinements such as thin film,[17−19] pore (cylindrical),[20−24] sphere,[20] and in systems that involve the inclusion of filler particles.[25] Most theoretical studies on block copolymers in thin films are focused on two-component systems, which are either AB diblock or symmetric ABA triblock copolymers.[26−29] Furthermore, the copolymers that form a hexagonal cylindrical structure in the bulk, in short of cylinder-forming AB[30−32] and ABA block copolymers,[27,33,34] are studied in detail.

Until now, few reports concentrate on ABC triblock terpolymer systems. This may be due to their greater quantities of chain architecture and interaction parameters. Naturally, the microphase separation of ABC triblock terpolymer systems will in general be more complicated than that of diblock because it is more possible to have three distinct interfaces instead of just one, and there are more stretching energy contributions with three distinct blocks rather than with just two.[5,35] On the other hand, ABC systems have the potential to become much more useful in nanofabrication than two-component systems because of the numerous distinct morphologies they possess.

Previous works on ABC triblock terpolymers thin films revealed that film thickness, surface field, and interaction parameters can be employed to manipulate microdomain structure, shape, and orientation.[36−39] The phase behavior of ABC triblock terpolymer in thin films, which exhibits a core−shell gyroid structure in the bulk, has been systematically studied by Ludwings et al. by both conducting experiments and using mesoscale simulations.[40,41] For a cylinder-forming ABC triblock terpolymer, a highly ordered hexagonally perforated lamella structure is formed irrespective of the preference of the substrate.[42] This property is superior over other systems that require considerable efforts concentrating on adjusting the substrate surface energy or the patterning technique for lithography to achieve the desired orientation of the nanostructure. As a study that combines experiment and simulation, this work[42] is only concerned with the perforated lamella structure; the effect of film thickness and surface field on the phase behavior of this cylinder-forming triblock terpolymer is beyond the scope of the study. It is interesting to investigate whether the confined cylinder-forming triblock terpolymer exhibits the same phase behavior as the diblock copolymer. Moreover, the additional middle block in the triblock terpolymer makes it different from the diblock copolymer in terms of chain configuration, and the effect that the surface field plays on the middle block of the triblock terpolymer is unique and does not exist in diblock systems. This paper tries to elaborate on such issues.

As the simulated system sizes are limited in simulations, the periodic boundary conditions (PBCs) are always employed for a bulk condition. It has been pointed out that for lattice simulations, this imposed periodicity may play artificial stresses on the structure, which could alter the period of the domain structure or even the structure itself.[31,43] The use of large simulation cells is a choice, but it is beyond the current computational capabilities of systems that cannot be simulated using a parallelization algorithm.[44] Wang et al. once successfully performed Monte Carlo simulations of cylinder-forming asymmetric diblock copolymer thin films in a grand canonical

* Corresponding author. E-mail: hjliang@ustc.edu.cn.
† Hefei National Laboratory for Physical Sciences at Microscale.
‡ Department of Polymer Science and Engineering.

10.1021/jp061957c CCC: $33.50
Published on Web 08/24/2006

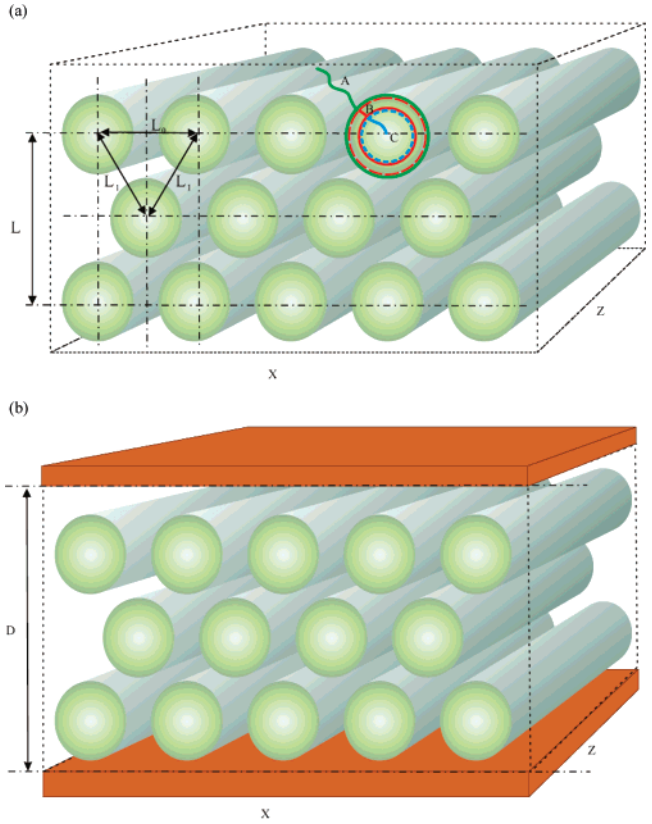

Figure 1. Schematic illustrations of the self-assembled triblock terpolymer system. (a) In the bulk. The core−shell structure is shown on the right cylinder with A, B, and C representing three blocks in a chain. L_0 is the cylinder period (the distance between the centers of the two nearest cylinders that are parallel to the box surface) in the bulk, and L_1 is the cylinder period next to L_0. L is the pattern period of the hexagonally arranged cylinders in the bulk. (b) In the film. D is the distance between top and bottom surfaces, that is, the film thickness. Lx and Lz are the lengths of the film in the x and z directions, respectively.

ensemble.[32] With a judicious choice of the simulation box size, the periodicity of the domain structure was matched with the PBCs in their simulations. This method is reasonable and has been used in the simulations of symmetric and asymmetric diblock copolymers.[31,32] The results are satisfactory and consistent with other calculations.[30]

In this work, we perform an extensive study of a cylinder-forming ABC triblock terpolymer in thin films using canonical ensemble Monte Carlo simulations. A simulated annealing mechanism is applied in the self-assembling process. This annealing method has been successfully applied in Monte Carlo simulations of block copolymers self-assembling in a solution and a confined system.[45,46] With suitable choice of the chain architecture and components interaction, the ABC triblock terpolymer exhibits a well-developed hexagonal cylinder phase embedded within the majority of block matrix in the bulk. The cylinder phase is compatible with the idea of the core−shell structure, where the C-block forms a cylindrical core surrounded by a B-block shell (see Figure 1a). The top and bottom surfaces are identical, homogeneous, and hard (see Figure 1b). Applying the judicious selection of simulation box dimensions as did Wang et al., we systematically studied the effect of film thickness and surface field on self-assembled morphologies.

To limit the scope of the study, we select a triblock terpolymer system that forms a hexagonally arranged cylindrical structure in the bulk, and then we change the film thickness under different surface fields. The rest of this paper is organized as follows. In section 2, we briefly describe the model and simulation method. In section 3, we present bulk simulation, and the cylinders period (L_0) and the pattern period (L) are estimated. In section 4, we briefly compare the simulation results of the triblock $A_{13}B_2C_3$ system in this study with the diblock $A_{15}C_3$ system. In section 5, we systemically study the phase behavior of the triblock $A_{13}B_2C_3$ system in the film: (5.1) the surfaces are neutral to all blocks, (5.2) the surfaces are preferred for the A-block, (5.3) the surfaces are preferred for the B-block, and (5.4) the surfaces are preferred for the C-block. Finally, in section 6, the conclusion of this paper is presented.

2. Model

2.1. Lattice Model. The Monte Carlo simulations used in this work are performed in a canonical ensemble in the framework of a simple cubic lattice.[20,21] Each monomer occupies one lattice site, and each lattice site is either vacant (also called unoccupied lattice site) or occupied by one monomer at most. We work in a constant monomer volume fraction of 70% (this means that 70% of all of the lattice sites are occupied by monomers) to reproduce a melt behavior in our simulations. All simulations are run in a three-dimensional box, and the lengths in the x, y, and z directions are Lx, Ly, and Lz, respectively. Two flat and homogeneous surfaces are introduced through the lattice sites at $y = 0$ and $y = Ly + 1$. These lattice sites are not allowed to be vacant or occupied by any monomer. To emphasize the distance between the two surfaces, we use D instead of Ly, as shown in Figure 1b. Periodic boundary conditions (PBCs) are imposed in the x and z directions. For simulations in the bulk, PBCs are also imposed in the y direction.

The triblock terpolymer is simulated using a chain with 18 monomers. The first N_A monomers are of type A noted as A-block; the second N_B monomers are of type B noted as B-block, which is the middle block in this work; and the last N_C monomers are of type C noted as C-block ($N_A + N_B + N_C = 18$). In the triblock terpolymer system, the chain architecture and interaction parameter are both very complicated. In this study, to obtain a core−shell cylinder structure in the bulk, we choose a chain architecture that is $A_{13}B_2C_3$ ($N_A = 13$, $N_B = 2$, and $N_C = 3$). The repulsions between different types are $\epsilon_{AC} = 1.0$, $\epsilon_{AB} = 0.1$, and $\epsilon_{BC} = 1.0$. In this parameter space, polymer A and polymer B are highly incompatible with polymer C, while the repulsion between polymer A and polymer B is relatively low. In this model, we simulate a chain with three distinct segments. To compare with the diblock copolymer system, in parts of bulk simulation and film simulation (in section 4), the interaction energy of monomer A and monomer B (ϵ_{AB}) is varied. We always set the interaction energies of the same type $\epsilon_{AA} = \epsilon_{BB} = \epsilon_{CC} = 0$, and those of monomers and vacancies (V) $\epsilon_{AV} = \epsilon_{BV} = \epsilon_{CV} = 0$. The surface (S)−polymer interaction energies such as ϵ_{SA}, ϵ_{SB}, and ϵ_{SC} are considered in different conditions, and $\epsilon_S = 0$ corresponds to the neutral surface ($\epsilon_{SA} = \epsilon_{SB} = \epsilon_{SC} = 0$).

The vacancy diffusion algorithm combined with the single-site bond fluctuation model (that is, the bond is 1 or $\sqrt{2}$ in the unit of lattice) is used in the move set. The evolution of chain configuration is achieved by a random displacement of a vacancy to a monomer in its neighboring sites only if no bond crossing occurs. The Metropolis Rule governs each step of the moving process. A movement try is accepted if the energy changes are less than zero; otherwise, it is accepted with a probability P of $\exp(-\Delta E/kT)$, where ΔE is the energy change of the movement, k is the Boltzmann constant (is set to 1 for simplicity), and T is the system temperature. The value of

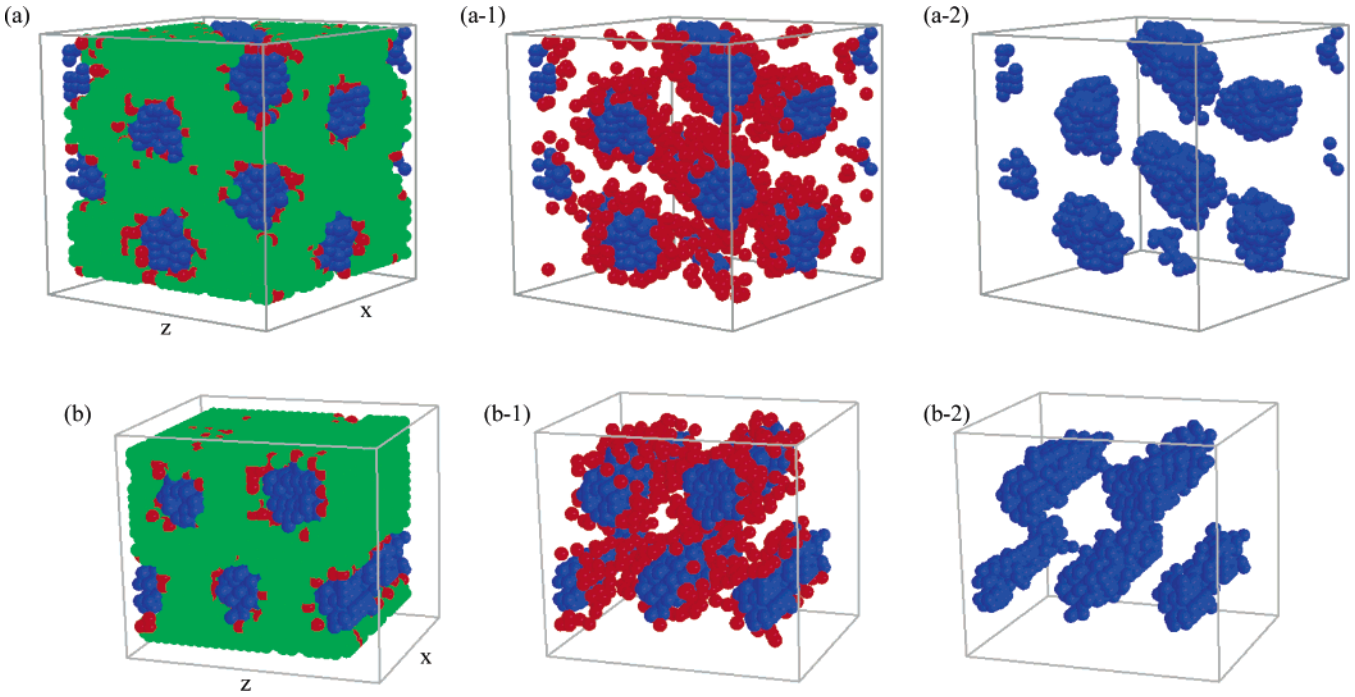

Figure 2. Self-assembled cylindrical structure of ABC triblock terpolymer in the bulk. The interaction parameters are $\epsilon_{AC} = 1.0$, $\epsilon_{AB} = 0.1$, and $\epsilon_{BC} = 1.0$. (a) The box dimensions $Lx \times Ly \times Lz$: $27 \times 28 \times 29$, all blocks are shown; (a-1) B- and C-blocks are shown; (a-2) only C-blocks are shown. (b) The box dimensions $Lx \times Ly \times Lz$: $24 \times 22 \times 25$, all blocks are shown; (b-1) B- and C-blocks are shown; (b-2) only C-blocks are shown.

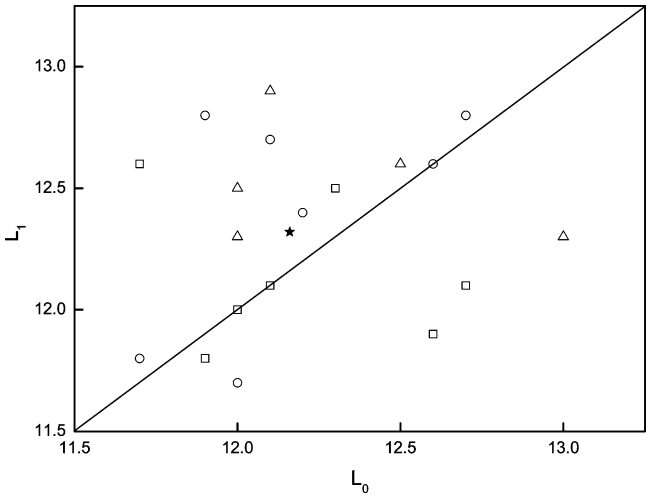

Figure 3. Bulk simulation results for different boxes. L_0 and L_1 are cylinder periods shown in Figure 1; open symbols with different shapes represent different box dimensions ($Lx \times Ly \times Lz$): □ represent $21 \times 24 \times 25$, ○ represent $22 \times 23 \times 24$, △ represent $24 \times 22 \times 25$, ★ represent the average value of all L_0 and L_1.

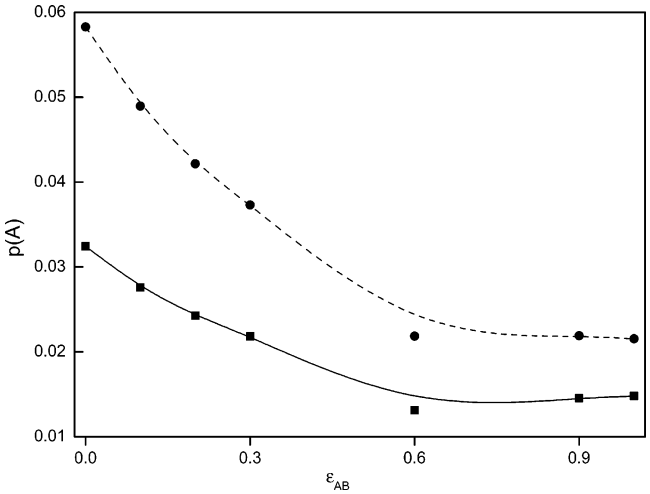

Figure 4. The distribution of the A-block circling around the C-block domain (p(A)) with different values of ϵ_{AB}. ■ refers to the p(A) of the entire C-block, which is in short of "all C", ● refers to the p(A) of the only segment of C-block that is next to the B-block, which is in short of "B−C".

ΔE is calculated as

$$\Delta E = (\Delta N_{AB}\epsilon_{AB} + \Delta N_{AC}\epsilon_{AC} + \Delta N_{BC}\epsilon_{BC} + \Delta N_{SA}\epsilon_{SA} + \Delta N_{SB}\epsilon_{SB} + \Delta N_{SC}\epsilon_{SC})$$

where ΔN is the difference between the number of pairs of neighboring sites occupied by monomers A, B, C, and the surface. One Monte Carlo step (MCS) consists of $0.7 \times Lx \times Ly \times Lz$ trials of movement.

2.2. Simulated Annealing Procedure. We apply a schedule of $T_{j+1} = fT_j$ in the stepwise annealing process, where T_j is the relaxation temperature at the jth annealing step, and f is the scaling factor. The annealing procedure involves that a homogeneous system runs from the initial temperature T_0 and reaches the equilibrium temperature T_f after predetermined N annealing steps. At each annealing step, the relaxation temperature is constant. In this work, the temperature begins at $T_0 = 10.0$ and reaches $T_f = 1.85$ after 17 steps ($f = 0.9$). At each annealing step, we perform at least 200 000 MCS.

2.3. Choice of Simulation Box Dimensions. The cylinder phase in our ABC triblock terpolymer system is similar to that in an asymmetric diblock copolymer system. Our approach is based on the study of Wang et al.,[32] so we abbreviate the detailed description. In the bulk simulation, we define L_0 and L_1 as the cylinder periods that represent the distance between the center of the two nearest cylinders in the bulk, and L (L_2 in ref 32) as the pattern period in the bulk, as shown in Figure 1a. The difference between L_0 and L_1 is that L_0 is the distance between the two nearest cylinders parallel to one surface of the box. In

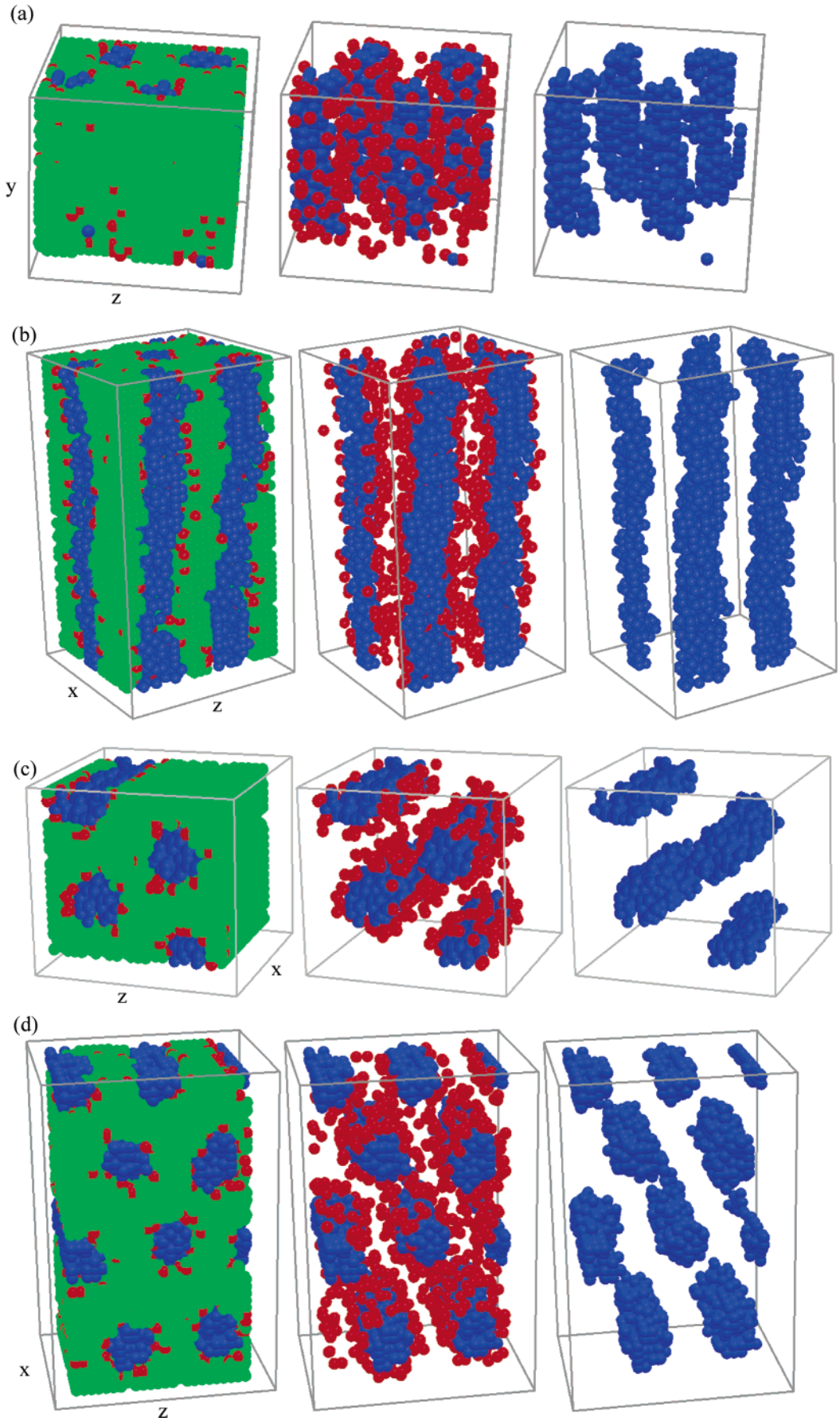

Figure 5. Self-assembled structures of the diblock $A_{15}C_3$ system and the triblock $A_{13}B_2C_3$ system under the weak surface field ($\epsilon_{SA} = -0.2$). From left to right, all blocks are shown first; then the B- and C-blocks are shown next; last, only C-blocks are shown. (a) The diblock $A_{15}C_3$ system with film thickness $D/L = 1$. (b) The diblock $A_{15}C_3$ system with film thickness $D/L = 2$. (c) The triblock $A_{13}B_2C_3$ system with film thickness $D/L = 1$. (d) The triblock $A_{13}B_2C_3$ system with film thickness $D/L = 2$.

TABLE 1: Self-Assembled Morphologies of ABC Triblock Terpolymer Thin Films[a]

D/L	neutral	$\epsilon_{SA} = -0.2$	$\epsilon_{SA} = -1$	$\epsilon_{SB} = -0.2$	$\epsilon_{SB} = -1$	$\epsilon_{SC} = -0.2$	$\epsilon_{SC} = -1$
0.25	$C_\perp$	$C_\perp$	W	$C_\perp$	$C_\perp$	$C_\perp$	W−W
0.5	$C_{\parallel}^{1/2}$−$C_{\parallel}^{1/2}$	$C_\perp$	$C_{\parallel}^{1}$	$C_{\parallel}^{1/2}$−$C_{\parallel}^{1/2}$	$C_{\parallel}^{1/2}$−$C_{\parallel}^{1/2}$	W−W	W−W
0.75	$C_\perp$	$C_\perp$	$C_{\parallel}^{1}$	$C_{\parallel}^{1/2}$+$C_\perp$	$C_{\parallel}^{1/2}$−$C_{\parallel}^{1/2}$	W−S−W	$L_{\parallel}$−$L_{\parallel}$
1	$C_{\parallel}^{1/2}$−$C_{\parallel}^{1}$−$C_{\parallel}^{1/2}$	$C_{\parallel}^{1/2}$−$C_{\parallel}^{2}$−$C_{\parallel}^{1/2}$	$C_{\parallel}^{2}$	$C_{\parallel}^{1/2}$−$C_{\parallel}^{1}$−$C_{\parallel}^{1/2}$	$C_{\parallel}^{1/2}$−$C_{\parallel}^{1}$−$C_{\parallel}^{1/2}$	W−$C_{\parallel}^{1}$−W	$L_{\parallel}$−S−$L_{\parallel}$
1.25	$C_{\parallel}^{1/2}$−$C_{\parallel}^{1}$−$C_{\parallel}^{1/2}$	$C_\perp$	$C_{\parallel}^{2}$	$C_{\parallel}^{1/2}$−$C_{\parallel}^{1}$−$C_{\parallel}^{1/2}$	$C_{\parallel}^{1/2}$−$C_{\parallel}^{1}$−$C_{\parallel}^{1/2}$	W−$C_{\parallel}^{1}$−W	$L_{\parallel}$−$C_{\parallel}^{1}$−$L_{\parallel}$
1.5	$C_{\parallel}^{1/2}$−$C_{\parallel}^{2}$−$C_{\parallel}^{1/2}$	$C_\perp$	$C_{\parallel}^{3}$	$C_{\parallel}^{1/2}$−$C_{\parallel}^{2}$−$C_{\parallel}^{1/2}$	$C_{\parallel}^{1/2}$−$C_{\parallel}^{2}$−$C_{\parallel}^{1/2}$	W−$C_{\parallel}^{2}$−W	$L_{\parallel}$−D−$L_{\parallel}$
1.75	$C_{\parallel}^{1/2}$−$C_{\parallel}^{2}$−$C_{\parallel}^{1/2}$	$C_\perp$	$C_{\parallel}^{3}$	$C_{\parallel}^{1/2}$−$C_{\parallel}^{2}$−$C_{\parallel}^{1/2}$	$C_{\parallel}^{1/2}$−$C_{\parallel}^{2}$−$C_{\parallel}^{1/2}$	W−$C_{\parallel}^{2}$−W	$L_{\parallel}$−$C_{\parallel}^{2}$−$L_{\parallel}$
2	$C_{\parallel}^{1/2}$−$C_{\parallel}^{3}$−$C_{\parallel}^{1/2}$	$C_{\parallel}^{1/2}$−$C_{\parallel}^{3}$	$C_{\parallel}^{4}$	$C_{\parallel}^{1/2}$−$C_{\parallel}^{3}$−$C_{\parallel}^{1/2}$	$C_{\parallel}^{1/2}$−$C_{\parallel}^{3}$−$C_{\parallel}^{1/2}$	W−$C_{\parallel}^{3}$−W	$L_{\parallel}$−$C_{\parallel}^{2}$−$L_{\parallel}$

[a] The parallel cylinder structure is signed as $C_{\parallel}^{n}$ with $n = {}^1/_2$ or an integer, half of a cylinder or the number of cylinders existing in the films along the y axis. The perpendicular cylinder structure is signed as $C_\perp$. A lamellar wetting layer of disordered structure is signed as W. S and $L_{\parallel}$ represent the spherical and lamellar structures, respectively. We use D to depict the distorted cylinder structure.

Figure 1a, the cylindrical morphology is parallel to the $x-z$ plane. In a regular-hexagonal pattern of the cylinder phase, $L = \sqrt{3}L_0$, and L_0 is equal to two values of L_1 (see ref 32 for details).

In the film simulation, there are two surfaces located in the $x-z$ plane that confine the polymer system. D is the distance between two surfaces in the y direction, which varies from $0.25L$ to $2L$ in both weak and strong surface field conditions in this study. The sides $Lx \times Lz$ are chosen as $L \times 2L_0$ or $2L \times 4L_0$ to match cylinders that are both perpendicular and parallel to the surfaces.[32]

2.4. Characterization of the Morphology. By using the simulated annealing procedure, the self-assembled morphologies are found to be less defective and independent of the starting configurations, as can be easily identified by visual inspection. We also monitor the ensemble-averaged density and orientation profiles along the y axis that is perpendicular to the surfaces. After equilibration, we collect 1000 successive configurations with the interval of five MCS. The density profiles ρ_A, ρ_B, and ρ_C, which refer to the percentages of occupied lattice sites by different monomers at a given y, are calculated along the y axis. The relative density profiles are calculated as $\langle \rho_{B(C)} - \rho_A \rangle$, which means that the density profile differences between the B- (or C-) block and the A-block in the cross section of the $x-z$ plane at a given y are ensemble-averaged over all collected configurations.

We define an orientation vector pointing from the center-of-mass of the A-block to the center-of-mass of the C-block in a chain. The ensemble-averaged $\langle|\cos\theta|\rangle$ and $\langle\cos\theta\rangle$ are calculated, where θ is the angle between the orientation vector of a chain and the y axis that is perpendicular to the surfaces. Furthermore, we use $\langle|\cos\theta|\rangle = (1/\pi)\int_0^\pi |\cos\theta|\, d\theta = 2/\pi$ as the criterion between the perpendicular and parallel orientations of the chains.[32] We note that if the chains are mainly parallel to the surfaces, $\theta \approx \pi/2$ and $\langle|\cos\theta|\rangle < 2/\pi$. If the chains are mainly perpendicular to the surfaces, $\theta \approx 0$ or π and $\langle|\cos\theta|\rangle > 2/\pi$.

3. Simulations in the Bulk

To decide the values of pattern period L in the bulk, we perform bulk simulations with different box dimensions ($Lx \neq Ly \neq Lz$). In different runs, the cylinder orientations and distances between cylinders are varied with each other, as Figure 2 shows. In the lattice simulation with limited box dimensions, it is hard to get a regular-hexagonal cylindrical structure, and it is difficult to equalize the values of L_0 and L_1, so we relax the condition and only require $|L_0 - L_1| < 1$. We choose three different boxes ($21 \times 24 \times 25$, $22 \times 23 \times 24$, $24 \times 22 \times 25$) to calculate L_0 and L_1, because most cylindrical morphologies in them are parallel to one of three surfaces. Hence, we can calculate the distances between the neighboring cylinders according to the lattice unit, as shown by the results in Figure 3. Although the values of L_0 and L_1 are varied from each other, most of them are concentrated in a narrow scope. We obtain the average values of $L_0 = 12.16$ and $L_1 = 12.32$, and so the pattern period $L = \sqrt{3}L_0 \approx 21$. The sides $Lx \times Lz$ in the thin

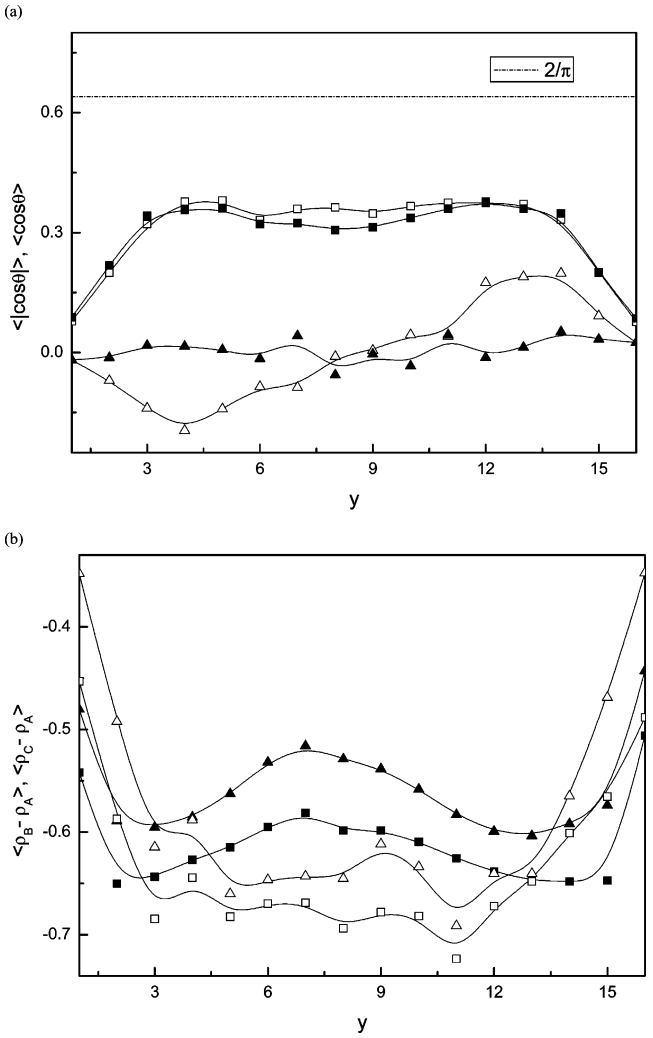

Figure 6. The profiles of the perpendicular cylindrical structure ($C_\perp$) with $D/L = 0.75$. The box size in the $x-z$ cross section is 21×24. (a) The chain orientation profiles: □ represents $\langle|\cos\theta|\rangle$ under neutral surfaces ($\epsilon_S = 0$), and △ represents $\langle\cos\theta\rangle$ under neutral surfaces ($\epsilon_S = 0$); ■ represents $\langle|\cos\theta|\rangle$ under the surfaces that slightly prefer A-block ($\epsilon_{SA} = -0.2$), and ▲ represents $\langle\cos\theta\rangle$ under the surfaces that slightly prefer A-block ($\epsilon_{SA} = -0.2$). (b) The relative density profiles: □ represents $\langle\rho_B - \rho_A\rangle$ under neutral surfaces ($\epsilon_S = 0$), and △ represents $\langle\rho_C - \rho_A\rangle$ under neutral surfaces ($\epsilon_S = 0$); ■ represents $\langle\rho_B - \rho_A\rangle$ under the surfaces that slightly prefer A-block ($\epsilon_{SA} = -0.2$), and ▲ represents $\langle\rho_C - \rho_A\rangle$ under the surfaces that slightly prefer A-block ($\epsilon_{SA} = -0.2$).

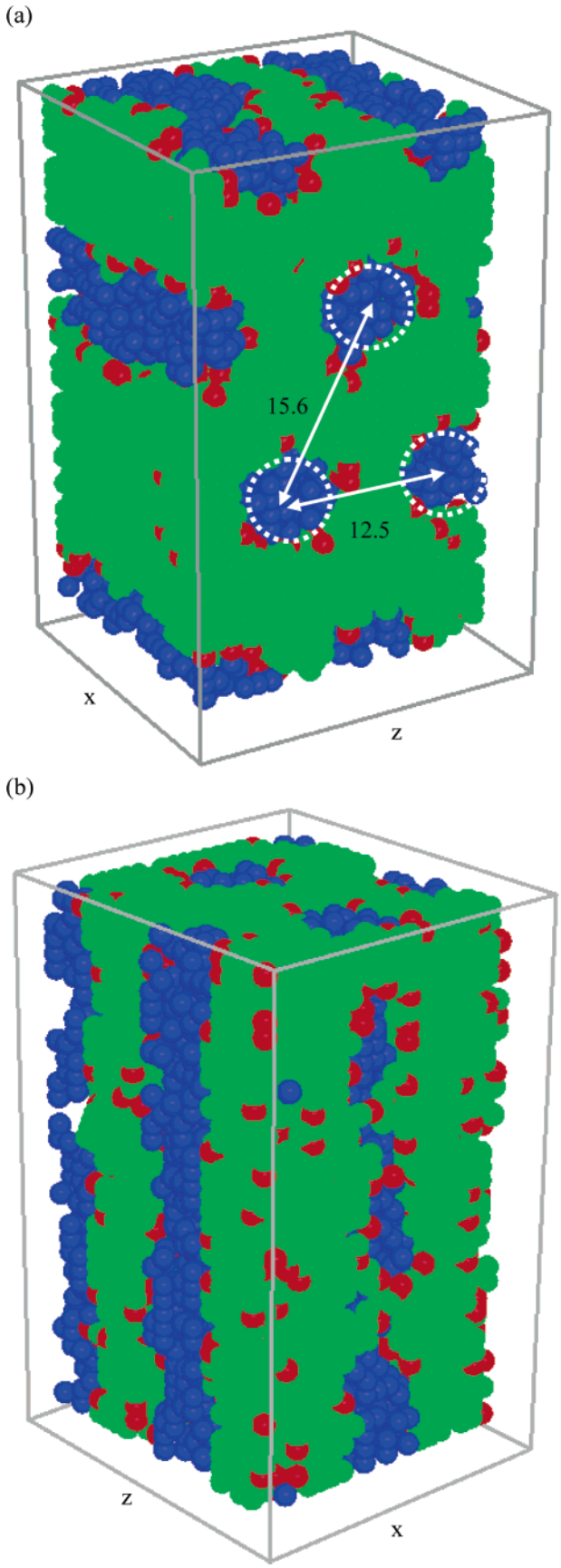

Figure 7. Self-assembled morphologies with $D/L = 1.75$ under different surface fields. The box size in the $x-z$ cross section is 21×24. (a) Parallel cylindrical structure $C_{\parallel}^{1/2}-C_{\parallel}^{2}-C_{\parallel}^{1/2}$ under neutral surfaces ($\epsilon_S = 0$), the cylinder period in the $x-z$ plane is 12.5 and that in the $y-z$ plane is 15.6. (b) Perpendicular cylindrical structure $C_{\perp}$ under the surfaces that slightly prefer A-block ($\epsilon_{SA} = -0.2$).

film simulation are chosen as 21×24 ($L \times 2L_0$) or 42×48 ($2L \times 4L_0$).

4. To Compare the $A_{13}B_2C_3$ Triblock Terpolymer System with the $A_{15}C_3$ Diblock Copolymer System

As Figure 2 shows, the ABC triblock terpolymer exhibits a well-developed hexagonal cylinder phase (minority B-block and C-block) embedded within the majority A-block matrix. It is very similar to the cylinder phases of the AB and ABA two-component systems in the bulk, and the only difference between them is a core (C-block)−shell (B-block) structure in the cylinder phase of the three-component system, as shown in Figure 1a. Because of the fact that the B-block is connected to the C-block in the chain architecture, the layer next to the C-domain will always be enriched by the B-block. It is hard to distinguish the triblock system from the diblock system only by this core−shell structure through visual inspection. However, the A-block must be repelled from the C-block domain by the B-block in the triblock system. Comparing the distribution of the A-block circling around the C-block domain in the triblock system with that in the diblock systems is an effective method to study the difference between the microstructures of the diblock and the triblock systems.

In our model, when $\epsilon_{AB} > 0$, it is a triblock terpolymer system; when $\epsilon_{AB} = 0$ in the $A_{13}B_2C_3$, the triblock terpolymer system changes into the $A_{15}C_3$ diblock copolymer system. To compare the microstructure of the cylinder-forming diblock copolymer system with that of the cylinder-forming triblock terpolymer system, we vary the interaction energy of polymer A with polymer B (ϵ_{AB}) from 0 to 1.0 in the bulk simulation with the same box dimensions: $27 \times 28 \times 29$. All of these bulk simulations start from the same homogeneous state, and the random number generator seeds are also the same. We got seven cylindrical morphologies at last; these are $\epsilon_{AB} = 0$, 0.1, 0.2, 0.3, 0.6, 0.9, 1.0. After equilibration, we collected 1000 successive configurations with an interval of five MCS. We calculated the ensemble-averaged distribution of the A-block circled around the C-block domain. The distribution of the A-block around the C-block domain is calculated as the possibility to find a monomer A in the neighboring sites of a monomer C, which is in short p(A). Because most C-blocks form the cores of cylinders in the system, we calculated p(A) around all three C-blocks (that is, "all C" in Figure 4). Moreover, because monomer C that is next to the B-block should always exist in the edge of the core, there should be more A-blocks revolving around it than the two other monomer C segments; we also calculated the p(A) around this single monomer C (that is, "B−C" in Figure 4). In the $A_{15}C_3$ diblock system, we only calculated the distribution of the first 13 monomers of the A-block in a chain. Hence, we avoided the architecture effect on p(A) in the diblock system, which would increase the p(A) in the diblock system.

As Figure 4 shows, the p(A) values in the diblock system are higher than those in the triblock system; in other words, there are less A-blocks in the layer next to the C-blocks domain in the triblock system in relation to those in the diblock system due to the repulsion of the B-blocks. Thus, the triblock system has a unique enriched B-block shell structure that does not exist in the diblock system. As ϵ_{AB} increases, the p(A) values diminish gradually when $\epsilon_{AB} < 0.6$, and they become less disturbed when $\epsilon_{AB} \geq 0.6$. When $\epsilon_{AB} = 0.1$, the p(A) difference of "all C" in $A_{13}B_2C_3$ in relation to that in $A_{15}C_3$ is about 0.01, and the p(A) difference of "B−C" in $A_{13}B_2C_3$ from that in $A_{15}C_3$ is about 0.005. When $\epsilon_{AB} = 0.6$, the p(A) difference of "all C" in

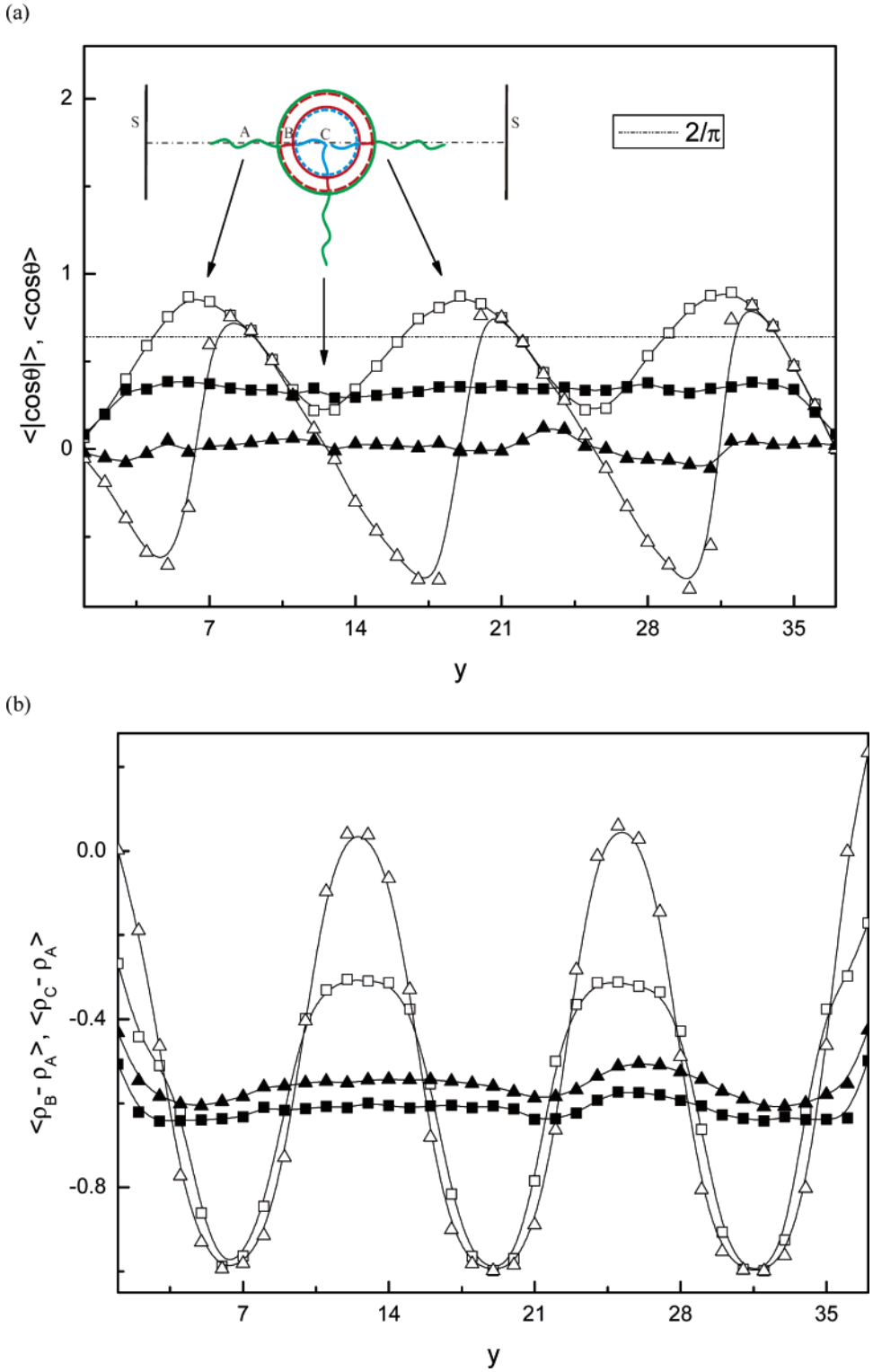

Figure 8. The profiles of parallel and perpendicular cylindrical structures with $D/L = 1.75$. The representative morphologies are shown in Figure 7a and b, respectively. (a) The chain orientation profiles: □ represents $\langle|\cos\theta|\rangle$ under neutral surfaces ($\epsilon_S = 0$), and △ represents $\langle\cos\theta\rangle$ under neutral surfaces ($\epsilon_S = 0$); ■ represents $\langle|\cos\theta|\rangle$ under the surfaces that slightly prefer A-block ($\epsilon_{SA} = -0.2$), and ▲ represents $\langle\cos\theta\rangle$ under the surfaces that slightly prefer A-block ($\epsilon_{SA} = -0.2$). The chain orientations are schematically represented in (a): A, B, and C represent three blocks, and S represents the surface. (b) The relative density profiles: □ represents $\langle\rho_B - \rho_A\rangle$ under neutral surfaces ($\epsilon_S = 0$), and △ represents $\langle\rho_C - \rho_A\rangle$ under neutral surfaces ($\epsilon_S = 0$); ■ represents $\langle\rho_B - \rho_A\rangle$ with the surfaces that slightly prefer A-block ($\epsilon_{SA} = -0.2$), and ▲ represents $\langle\rho_C - \rho_A\rangle$ under the surfaces that slightly prefer A-block ($\epsilon_{SA} = -0.2$).

$A_{13}B_2C_3$ from that in $A_{15}C_3$ is about 0.036, and the p(A) difference of "B−C" in $A_{13}B_2C_3$ from that in $A_{15}C_3$ is about 0.019. As a result, in the bulk, the microstructure of the $A_{13}B_2C_3$ system with $\epsilon_{AB} = 0.1$ is more similar to that of the $A_{15}C_3$ system as compared to the $A_{13}B_2C_3$ system with $\epsilon_{AB} \geq 0.6$. Thus, we may suppose that the $A_{13}B_2C_3$ system with $\epsilon_{AB} = 0.1$ may act like an $A_{15}C_3$ system in some degrees; as ϵ_{AB} increases, the phase behavior of the triblock is much more deviated as compared to that of the diblock system.

To compare the phase behaviors of the $A_{13}B_2C_3$ system with $\epsilon_{AB} = 0.1$ and the $A_{15}C_3$ system in the film, we also perform film simulations under the surface field $\epsilon_{SA} = -0.2$, which is

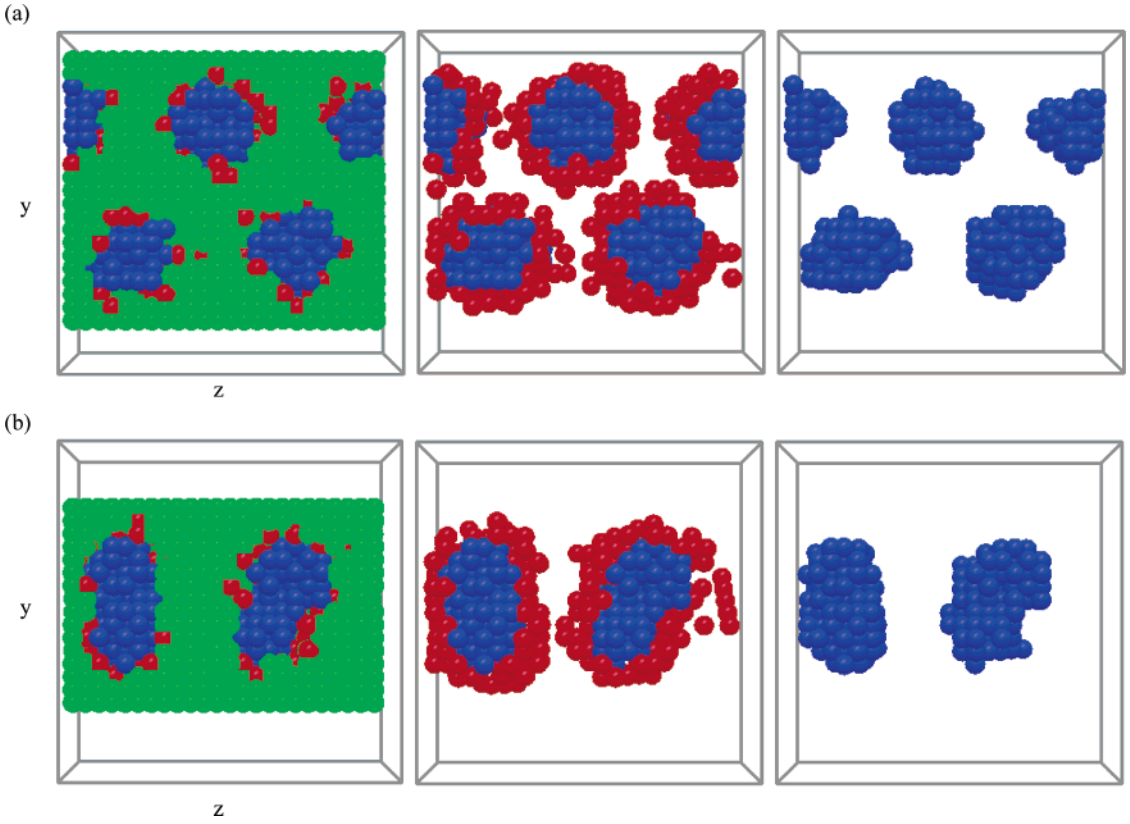

Figure 9. Two representative parallel cylindrical structures under the surfaces strongly prefer A-block ($\epsilon_{SA} = -1.0$). The box size in the $x-z$ cross section is 21×24. From left to right, all blocks are shown first, and then B- and C-blocks are shown; last, only C-blocks are shown. (a) $D/L = 1$; (b) $D/L = 0.75$.

a weak surface field. In most cases of film thickness, the perpendicular cylindrical morphologies are both observed in the diblock and triblock system. However, with the film thicknesses $D/L = 1$ and $D/L = 2$ for the $A_{15}C_3$ system, there are perpendicular cylindrical morphologies, as Figure 5a,b shows; for the $A_{13}B_2C_3$ system with $\epsilon_{AB} = 0.1$, the self-assembled structures are parallel cylindrical morphologies, as Figure 5c,d shows. Such a variation of cylinder orientation shows that, although the microstructures of the diblock system and triblock systems are similar in the bulk, the triblock terpolymer $A_{13}B_2C_3$ system with $\epsilon_{AB} = 0.1$ exhibits a different phase behavior in relation to that of the $A_{15}C_3$ diblock system in the film.

In the following section, we discuss the film simulations of the triblock terpolymer system in detail. For simplicity, we only concentrate on this $A_{13}B_2C_3$ system with $\epsilon_{AB} = 0.1$. We expect that such a system could retain some characterizations of the diblock system, which would help give us some clues on how the additional middle block affects the entire chain's behavior.

5. Simulations in Confined Films

Both frustration effect by confinement and the surface field play important roles in a polymer self-assembly process. To distinguish them, we consider the neutral surfaces ($\epsilon_S = 0$) to study the confinement effect. Next, the surfaces that are preferred for one of the three blocks are considered. For simplicity, we only consider the weak (-0.2) and the strong (-1.0) preference cases, and the surfaces prefer only one block at the separate condition. For examples, the surfaces that have a weak preference for C-block mean $\epsilon_{SC} = -0.2$, $\epsilon_{SA} = 0$, and $\epsilon_{SB} = 0$; and the surfaces that have a strong preference for A-block mean $\epsilon_{SA} = -1.0$, $\epsilon_{SB} = 0$, and $\epsilon_{SC} = 0$. The observed morphologies are summarized in Table 1.

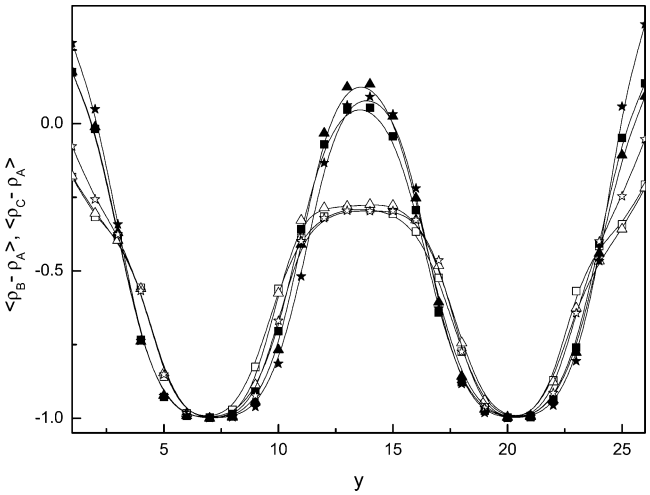

Figure 10. The relative density profiles of parallel cylindrical structures $C_{II}^{1/2}-C_{II}^{1}-C_{II}^{1/2}$ with $D/L = 1.25$ under neutral surfaces ($\epsilon_S = 0$), the surfaces that slightly prefer B-block ($\epsilon_{SB} = -0.2$), and the surfaces that strongly prefer B-block ($\epsilon_{SB} = -1.0$). □ and ■ represent $\langle \rho_B - \rho_A \rangle$ and $\langle \rho_C - \rho_A \rangle$ under neutral surfaces ($\epsilon_S = 0$), respectively; △ and ▲ represent $\langle \rho_B - \rho_A \rangle$ and $\langle \rho_C - \rho_A \rangle$ under the surfaces that slightly prefer B-block ($\epsilon_{SB} = -0.2$), respectively; ☆ and ★ represent $\langle \rho_B - \rho_A \rangle$ and $\langle \rho_C - \rho_A \rangle$ under the surfaces that strongly prefer B-block ($\epsilon_{SB} = -1.0$), respectively.

5.1. For Neutral Surfaces. When the surfaces are neutral, there is no preferential wetting for any block. Because D/L is an integer or half an integer, the pattern period of cylinder structure in the bulk is not or less frustrated, and the parallel cylinder phase (C_{II}) formed in the cases of $D/L = 0.5$, 1, 1.5, and 2. When D is highly incommensurate with the pattern period L (such as $D/L = 0.25$ and 0.75), the cylinder structure adopts a perpendicular orientation ($C_{\perp}$). For $D/L \leq 1$, the phase

behavior for the triblock terpolymer system is the same as that for the diblock copolymer system.[32] On the other hand, for $D/L = 1.25$ and 1.75, there are parallel cylinders other than perpendicular cylinders; these are different from the diblock copolymer.[32] Suh et al. once presented a theoretical study on the ordering of cylindrical morphology in diblock and triblock copolymer thin films.[47] They concluded that the film thickness range in which the vertical morphology exists is not continuous; it jumps from one range to another as the thickness increases. Furthermore, the range decreases with increasing thickness, and the vertical morphology does not form for thick films. These conjectures are consistent with the phase diagram of an $A_3B_{12}A_3$ block copolymer film within the range of neutral and weak surface fields (see ref 33 in Figure 3). In the diblock copolymer system,[32] perpendicular cylinders were still observed when $D/L = 1.25$ and 1.75. This gives us the idea that the perpendicular cylinder phase range in a triblock terpolymer system decreases faster than that in a diblock system.

Because the cylinder structure with pattern period L develops spontaneously in the bulk, the interfacial energies between domains are most favored considering chain conformational entropy. Any frustration to this pattern period would increase the system's free energy, unless such increased energy is released by the environment. It has been shown that when asymmetric diblock copolymers are confined in a film, the neutral surfaces have a slight preference for the shorter block,[30,32] which is orientated to the surfaces. Hence, the parallel cylinder phase is preferred over the perpendicular phase when the system experiences no or less frustration. However, if the pattern period L is highly frustrated, the system's free energy would increase due to the stretching or compression of the polymer chains. As a result, the cylinder phase adopts a perpendicular orientation to reduce the stress on the polymer chains and make least the deformation of pattern period and cylinder structure. As shown in Figure 6, the slight preference of neutral surfaces for both shorter blocks (B-block and C-block) in the triblock terpolymer system can be observed. Although the surfaces are strictly neutral and the chains are mainly parallel to the surfaces particularly in the vicinity of surfaces (Figure 6a), there is obvious gathering for B- and C-blocks in the vicinity of the surfaces in relation to those far from the surfaces (Figure 6b). Meanwhile, for cylinders that are parallel to the surfaces, the cylinder period that is along the y axis is stretched to form half cylinders in the vicinity of the surfaces (Figure 7a), which would increase the system's free energy. However, it is an equilibrium state between the neutral surfaces, and the only energy compensation is due to the surface preference for B- and C-blocks. Although there are no such assertions in ABA triblocks[33] and other asymmetric triblock systems, we suppose that the preferential wetting of the strictly neutral surface for shorter blocks is common in all asymmetric systems.

An inspection of ensemble-averaged orientation profiles gives us a deep understanding of the arrangement of molecular chains. As Figure 6a shows, in a perpendicular cylindrical structure, the chains in the vicinity of the surfaces are more strictly parallel to the surfaces due to the hard-surface effect. For a parallel cylindrical structure, the orientations of chains circling around the cylinder center are shown in Figure 8a.

5.2. The Surfaces Preferred for A-Block. As shown in Table 1, when the surfaces have a slight preference for A-block (majority component), that is, $\epsilon_{SA} = -0.2$, perpendicular cylinder phases are more favored than parallel cylinder phases in most cases other than those when D/L are integers. The reason may be ascribed to the fact that the preference of neutral surface for shorter blocks is weakened by the surface field that prefers the majority component. Any frustration to the pattern period L that increases the free energy would orient the cylinders perpendicular to the surfaces. When D/L is an integer, there is no frustration to pattern period L, and so parallel cylindrical structure is preferred. When $D/L = 1$, there are one and a half cylinders in the planes perpendicular to the surfaces (Figure 5c) just like that in the $1.5C_{\parallel}$ structure in a recent SCFT study;[48] when $D/L = 2$, there are three and a half cylinders parallel to the surfaces, as Figure 5d shows. In the diblock system, the perpendicular cylinders are readily observed irrespective of the D/L value in ref 32. In the scope of our study, perpendicular cylindrical morphologies are always observed in the diblock $A_{15}C_3$ system. In the triblock $A_{13}B_2C_3$ system, perpendicular cylindrical morphology is observed when the pattern period L is frustrated (D/L is not an integer). Figure 5 shows that when D/L is an integer (1 or 2), the diblock $A_{15}C_3$ systems exhibit perpendicular cylindrical morphology, and the triblock $A_{13}B_2C_3$ systems exhibit parallel cylindrical morphology.

As Figure 6 shows, for a perpendicular cylinder structure, a weak surface field $\epsilon_{SA} = -0.2$ showed little influence on the

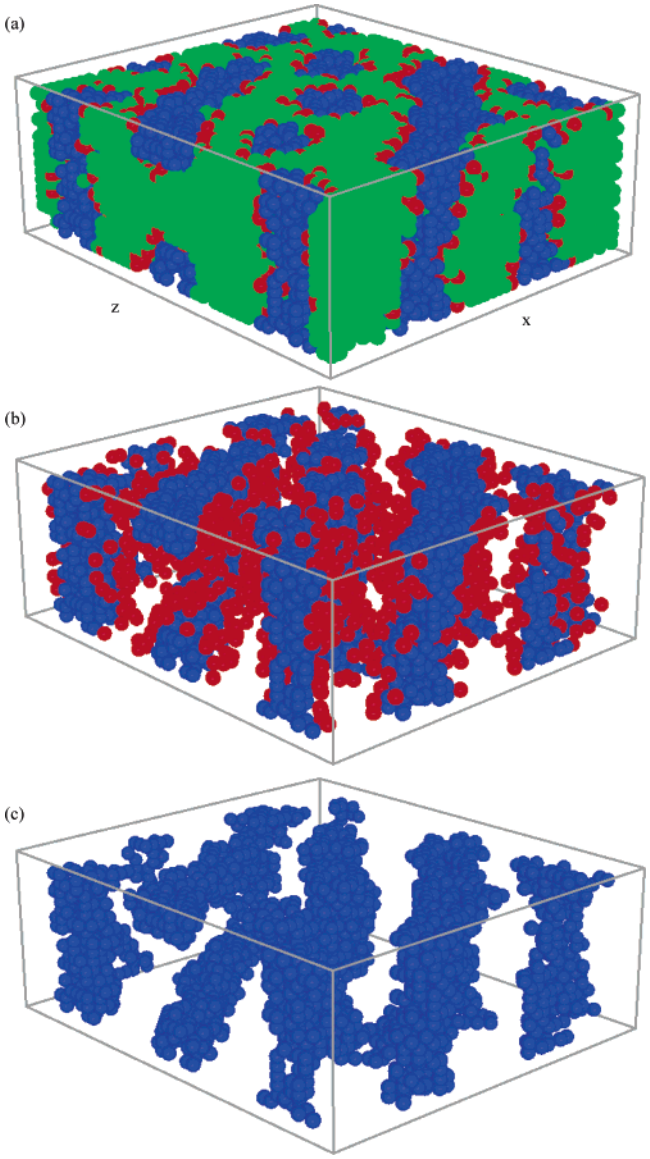

Figure 11. The mixed morphology of $C_{\parallel}^{1/2}+C_{\perp}$ with $D/L = 0.75$ under the surfaces that slightly prefer B-block ($\epsilon_{SB} = -0.2$). The box size in the $x-z$ cross section is 42×48. (a) All blocks are shown; (b) B- and C-blocks are shown; (c) only C-blocks are shown.

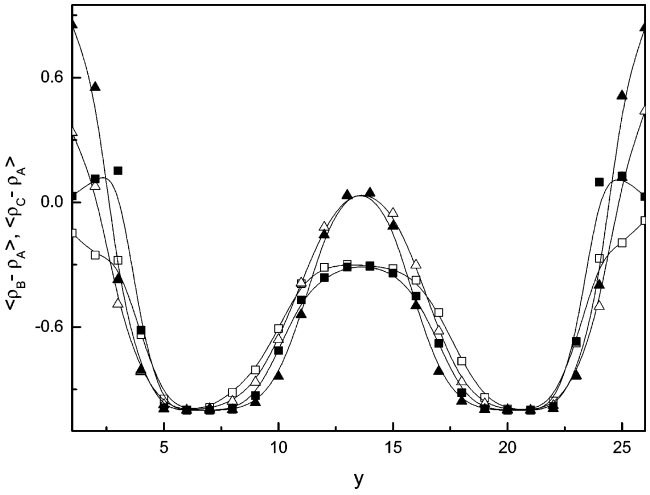

Figure 12. The relative density profiles with $D/L = 1.25$ under the surfaces preferred for C-block. □ and △ represent $\langle\rho_B - \rho_A\rangle$ and $\langle\rho_C - \rho_A\rangle$ under the surface field $\epsilon_{SC} = -0.2$, respectively, that is, W−$C_{||}^1$−W in Table 1; ■ and ▲ represent $\langle\rho_B - \rho_A\rangle$ and $\langle\rho_C - \rho_A\rangle$ under the surface field $\epsilon_{SC} = -1.0$, respectively, that is, $L_{||}$−$C_{||}^1$−$L_{||}$ in Table 1.

chains orientations, whereas it obviously decreased the quantity of minority components in the vicinity of the surfaces.

For a parallel cylinder structure where D is incommensurate with L (as $D/L = 1.75$ in Figure 7a), the weak surface field $\epsilon_{SA} = -0.2$ repels many minority components from the surfaces and orients the chains parallel to the surfaces (Figure 8). As a result, a perpendicular cylindrical structure (Figure 7b) forms instead of the parallel cylindrical structure (Figure 7a).

It is interesting to find a strong surface field ($\epsilon_{SA} = -1.0$) that orients cylinders parallel to the surfaces in most cases of D/L in the scope of our study. Only a very thin film ($D/L = 0.25$) displays no lateral structure, which is indicated by the term of a lamellar wetting layer (W); see Figure 13a. In two-component systems, a strong surface field for the majority of the components produced the lamellae, perforated lamellae, parallel cylinder, perpendicular cylinder, mixed cylinder structures, etc.[30,32] Regarding a gyroid-forming ABC triblock terpolymer system, there is also no single phase area observed.[41] We explain this unique phenomenon in our simulations considering the following: (1) the A-block is very long, and a screening effect forms as the surfaces are completely occupied by A-block ends, so the rest of the chain is less disturbed by the surface field; (2) the surface field is strong enough that there is no depletion of B- and C-blocks at surfaces, and consequently there are enough B- and C-blocks to form the regular core−shell cylinder structure; and (3) the B-block that resides between A-block and C-block would diminish the interfacial energy between the A-block domain and the C-block domain. Therefore, the preferred interfacial curvature for the C-block domain is preserved, making the triblock terpolymer system have a great capability to keep a well-ordered cylinder phase as compared to the two-component system.

To keep the cylinder structure in this triblock terpolymer system, not only the cylinder period (or pattern period) can be changed but also the cylinder radius and shape are flexible and adjust themselves to film thickness. When D and L are commensurate such as $D/L = 1$, a hexagonal arrangement of the circle cylinder structure develops in the film (Figure 9a). As $D/L = 0.75$, which is incommensurate with the cylinders period, the cylinders deform and turn elliptical (Figure 9b).

5.3. The Surfaces Preferred for B-Block. It seems that changing the strength of the surface field preferred for B-block has little influence on the thin film structures. As Table 1 shows, there is not much difference between the phase diagram of $\epsilon_{SB} = -0.2$ and that of $\epsilon_{SB} = -1.0$. This is because the B-block is a middle component, and the surface field that attracts the B-block would draw the C- and A-blocks that belong to the same chain by a geometric connection. Because the A-block is much longer than the C-block and so A-block experiences much more volume repulsion than C-block, the surface field thus shows pseudo preference for C-block as compared to A-block. The consequence is that the surfaces act like neutral surfaces with a stronger preference for minority components B- and C-blocks. As shown in Figure 10, a weak surface field ($\epsilon_{SB} =$

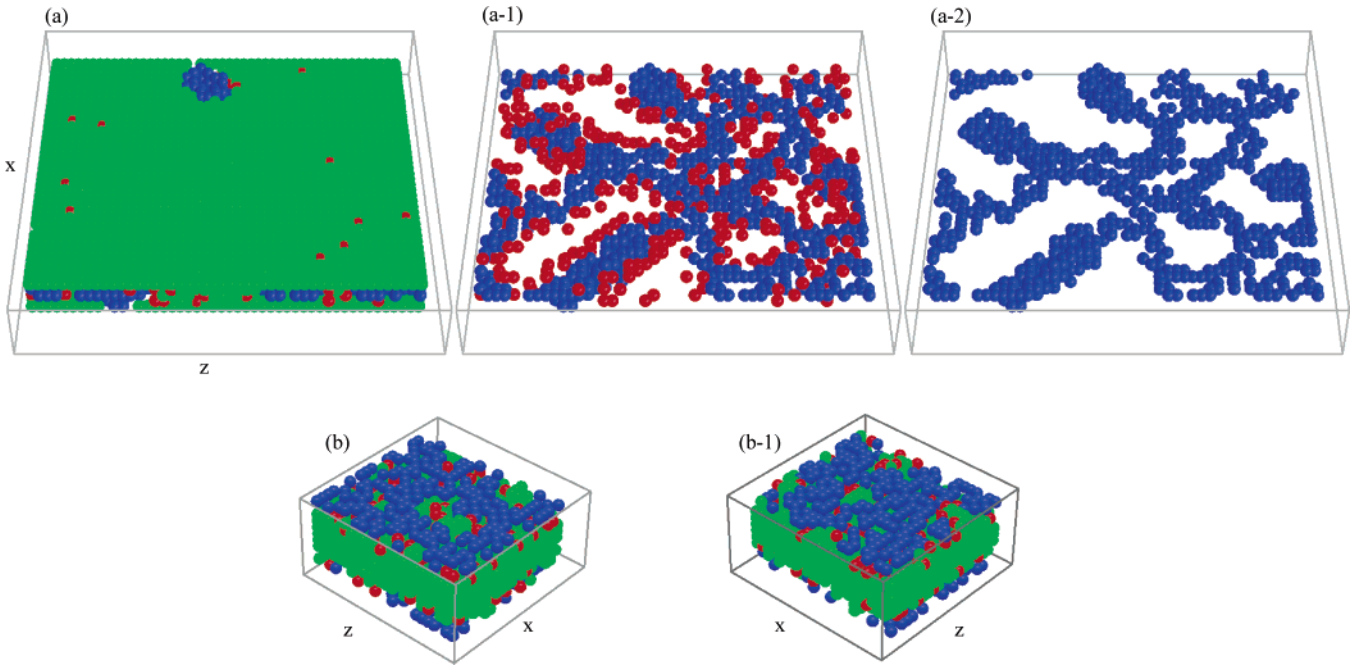

Figure 13. Representative W and W−W structures. (a) W structure under surface field $\epsilon_{SA} = -1.0$, the film thickness $D/L = 0.25$; (a-1) B- and C-blocks are shown; (a-2) only C-blocks are shown. (b) W−W structure under surface field $\epsilon_{SC} = -1.0$, the film thickness $D/L = 0.5$; the top interface is shown; (b-1) the bottom interface is shown, that is, the (b) is overturned.

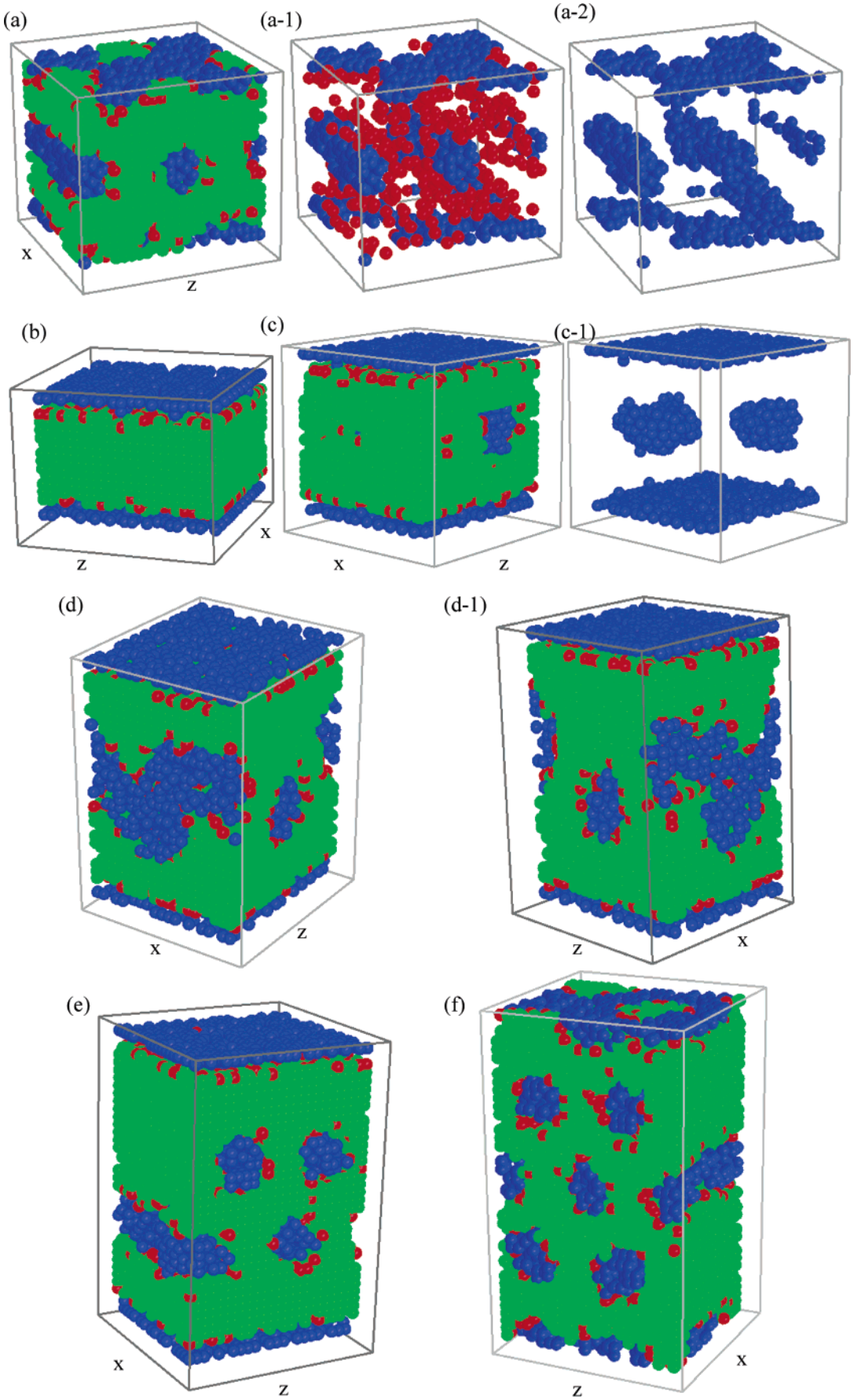

Figure 14. Representative morphologies between the surfaces being preferred for C-block. (a) W−$C_{||}^{1}$−W ($D/L = 1$, $\epsilon_{SC} = -0.2$); (a-1) B- and C-blocks are shown; (a-2) only C-blocks are shown. (b) $L_{||}$−$L_{||}$ ($D/L = 0.75$, $\epsilon_{SC} = -1.0$). (c) $L_{||}$−S−$L_{||}$ ($D/L = 1$, $\epsilon_{SC} = -1.0$); (c-1) only the C block is shown. (d) $L_{||}$−D−$L_{||}$ ($D/L = 1.5$, $\epsilon_{SC} = -1.0$); (d-1) rotate 90° from right to left around the *y* axis. (e) $L_{||}$−$C_{||}^{2}$−$L_{||}$ ($D/L = 1.75$, $\epsilon_{SC} = -1.0$). (f) W−$C_{||}^{3}$−W ($D/L = 2$, $\epsilon_{SC} = -0.2$). All box sizes in the $x-z$ cross section are 21×24.

-0.2) has little influence on the density profiles of B- and C-blocks, and a strong surface field ($\epsilon_{SB} = -1.0$) raises both the density profiles of B- and C-blocks at the surfaces. When $D/L = 0.75$ in Table 1, a mixed structure of perpendicular and parallel cylinders when $\epsilon_{SB} = -0.2$ is shown in Figure 11, which testifies that the surfaces show a stronger preference for B- and C-blocks than do the neutral surfaces. When the surface field is strong enough such that $\epsilon_{SB} = -1.0$, a parallel cylindrical structure is formed.

As Suh et al. pointed out, a perpendicular cylinder structure in very thin films is energy favored,[47] and so the orientation of cylinders is hard to be disturbed. In our simulations, for $D/L = 0.25$, the perpendicular cylinders are the most common case. Any strong surface field (such as $\epsilon_{SA} = -1.0$ and $\epsilon_{SC} = -1.0$ in Table 1) that reorients the cylinders turns the system into a disordered structure (Figure 13). As for the surfaces that prefer B-block, the perpendicular cylinders are undisturbed in a very thin film ($D/L = 0.25$).

5.4. The Surfaces Preferred for C-Block. Because the C-block is one of the chain ends, it can move more freely than the B-block. When the C-block is attracted by the surfaces, it can repel the other blocks in the vicinity of the surfaces. Although the C-block would draw the B-block by a geometric connection just like what the B-block does, the chain could orient itself perpendicularly to the surfaces, thereby reducing the B-block in the vicinity of the surfaces. As Figure 12 shows (please refer to Figure 10 for density profiles between the neural surfaces), the density profiles of the C-block at the surfaces increased obviously in relation to those of the B-block. For example, $\langle \rho_C - \rho_A \rangle$ at the surface $y = 1$ changed from 0.1745 ($\epsilon_S = 0$) to 0.3362 ($\epsilon_{SC} = -0.2$) and then 0.8536 ($\epsilon_{SC} = -1.0$), and for $\langle \rho_B - \rho_A \rangle$, there was a little increase from -0.1819 ($\epsilon_S = 0$) to -0.1472 ($\epsilon_{SC} = -0.2$). The dramatic change in $\langle \rho_B - \rho_A \rangle$ is that under a strong surface field ($\epsilon_{SC} = -1.0$), the maximum points of B-block density profiles move away from the surfaces to the $x-z$ planes, $y = 3$ and $y = 24$. For $y = 3$, the maximum point of $\langle \rho_B - \rho_A \rangle$ is 0.1519. Hence, the surfaces are mainly occupied by the C-block when the surfaces prefer it.

If the surface field is weak that it cannot attract enough C-blocks in the vicinity of the surfaces, or the film is very thin that the C-blocks cannot form a complete lamella, a disordered lamellar wetting layer of C-blocks at the surface is formed. In terms of the W−W structure with $D/L = 0.25$ and 0.5, two C-block lamellar wetting layers are formed at the surfaces. The representative structure is shown in Figure 13b. As film thickness increased, a series of interior structures form in the films as Table 1 shows. A typical $W-C_{||}{}^{1}-W$ structure is shown in Figure 14a. A regular lamella structure of the C-block at the surfaces forms under a strong surface field with the film thickness $D/L = 0.75$ as Figure 14b shows. Because the surface field depletes the component C at the surfaces, the other C-blocks in the film that could not form a cylinder structure form a spherical structure in the films as Figure 14c shows. In Table 1, a distorted cylinder structure ($L_{||}-D-L_{||}$) appears between the film thickness for a monolayer cylinder and that for a double layer cylinder structure, as shown in Figure 14d. In this structure, there are two C-block lamella at the surfaces and a layer of zigzag tilted cylinders parallel to the surfaces in the film interior. Such a distorted cylinder structure formed as a settlement of monolayer of cylinders and double layers of cylinders. However, this distorted cylinder structure may be a long-lived transient structure to a parallel cylindrical structure, or a hybrid of perpendicular cylinders with parallel cylinders. This should be explored by experiment or other theory studies. For the film that is thick enough, a hexagonally arranged parallel cylinder structure formed. When the surface field is strong, the cylinders are formed between two C-block lamella as Figure 14e shows; when the surface field is weak, the cylinders are formed between two C-block lamellar wetting layers as Figure 14f shows.

6. Conclusion

We studied the self-assembly morphologies of cylinder-forming ABC triblock terpolymer thin films by means of canonical ensemble Monte Carlo simulations. The film thickness and surface field is systematically considered, and much difference between the ABC triblock terpolymer system and the two-component cylinder-forming system is found. (1) Although the perpendicular cylinder structures are both favorable for thin films of the triblock terpolymer system and the two-component system when a parallel cylindrical structure is frustrated, the range for this vertical structure in the triblock terpolymer system decreases faster than that in a diblock copolymer system. (2) Because of the additional middle block B component in a chain, it is observed that the triblock terpolymer system has a great capability to keep a well-ordered cylinder structure. Also, the phase behavior of the cylinder-forming triblock terpolymer system varies differently from that of the diblock copolymer system. (3) We did not observe the perforated lamella phase when the surfaces prefer only one block. A previous study of cylinder-forming triblock terpolymer thin film revealed that the perforated lamella phase can be stabilized by a surface field with a certain film thickness.[42] Their study is different from our study in such a way that the surfaces they used have an effect on at least two components in their parameter space, which could break up the cylinder structure, whereas we consider only the cases in which the surfaces prefer only one block. Therefore, to control the surfaces being preferred for only one block is an effective way to control the cylinder's orientation in a triblock terpolymer thin film, at the same time retaining a regular cylindrical structure. When the surfaces prefer at least two blocks at the same time, or the top and bottom surfaces are distinct and prefer different blocks, the surface field would break up the cylinder structure, and a variety of noncylindrical structures would be favored.

Acknowledgment. We are grateful for the financial support provided by the Outstanding Youth Fund (No. 20525416), the Programs of the National Natural Science Foundation of China (Nos. 20490220, 20374050, and 90403022), and the National Basic Research Program of China (No. 2005CB623800).

References and Notes

(1) Bates, F. S.; Fredrickson, G. H. *Annu. Rev. Phys. Chem.* **1990**, *41*, 525.

(2) Mansky, P.; Chaikin, P.; Thomas, E. L. *J. Mater. Sci.* **1995**, *30*, 1987.

(3) Hamley, I. W. *Nanotechnology* **2003**, *14*, R39.

(4) Park, M.; Harrison, C.; Chaikin, P. M.; Register, R. A.; Adamson, D. H. *Science* **1997**, *276*, 1401.

(5) Bates, F. S.; Fredirckson, G. H. *Phys. Today* **1999**, *52*, 32.

(6) Shin, K.; Xiang, H.; Moon, S. I.; Kim, T.; McCarthy, T. J.; Russell, T. P. *Science* **2004**, *306*, 76.

(7) Xiang, H.; Shin, K.; Kim, T.; Moon, S. I.; McCarthy, T. J.; Russell, T. P. *Macromolecules* **2005**, *38*, 1055.

(8) Wu, Y.; Cheng, G.; Katsov, K.; Sides, S. W.; Wang, J.; Tang, J.; Fredrickson, G. H.; Moskovits, M.; Stucky, G. D. *Nat. Mater.* **2004**, *3*, 816.

(9) Walton, D. G.; Kellogg, G. J.; Mayes, A. M.; Lambooy, P.; Russell, T. P. *Macromolecules* **1994**, *27*, 6225.

(10) Kellogg, G. J.; Walton, D. G.; Mayes, A. M.; Lambooy, P.; Russell, T. P.; Gallagher, P. D.; Satija, S. K. *Phys. Rev. Lett.* **1996**, *76*, 2503.
(11) Tsori, Y.; Andelman, D. *J. Chem. Phys.* **2001**, *115*, 1970.
(12) Pereira, G. G. *Curr. Appl. Phys.* **2004**, *4*, 255.
(13) Xiang, H.; Shin, K.; Kim, T.; Moon, S. I.; McCarthy, T. J.; Russell, T. P. *Macromolecules* **2004**, *37*, 5660.
(14) Xu, T.; Hawker, C. J.; Russell, T. P. *Macromolecules* **2005**, *38*, 2802.
(15) Wang, Q. *Macromol. Theory Simul.* **2005**, *14*, 96.
(16) Stoykovich, M. P.; Muller, M.; Kim, S. O.; Solak, H. H.; Edwards, E. W.; de Pablo, J. J.; Nealey, P. F. *Science* **2005**, *308*, 1442.
(17) Masten, M. W. *J. Chem. Phys.* **1997**, *106*, 7781.
(18) (a) Geisinger, T.; Muller, M.; Binder, K. *J. Chem. Phys.* **1999**, *111*, 5241. (b) Geisinger, T.; Muller, M.; Binder, K. *J. Chem. Phys.* **1999**, *111*, 5251.
(19) Lambooy, P.; Russell, T. P.; Kellogg, G. J.; Mayes, A. M.; Gallagher, P. D.; Satija, S. K. *Phys. Rev. Lett.* **1994**, *72*, 2899.
(20) He, X. H.; Song, M.; Liang, H. J.; Pan, C. Y. *J. Chem. Phys.* **2001**, *114*, 10510.
(21) Chen, P.; He, X. H.; Liang, H. J. *J. Chem. Phys.* **2006**, *124*, 104906.
(22) Xiang, H.; Shin, K.; Kim, T.; Moon, S.; Mccarthy, T. J.; Russell, T. P. *J. Polym. Sci., Part B: Polym. Phys.* **2005**, *43*, 3377.
(23) Sevink, G. J. A.; Zvelindovsky, A. V.; Fraaije, J. G. E. M.; Huinink, H. P. *J. Chem. Phys.* **2001**, *115*, 8226.
(24) Sun, Y.; Steinhart, M.; Zschech, D.; Adhikari, R.; Michler, G. H.; Gosele, U. *Macromol. Rapid Commun.* **2005**, *26*, 369.
(25) Sevink, G. J. A.; Zvelindovsky, A. V.; van Vlimmeren, B. A. C.; Maurits, N. M.; Fraaije, J. G. E. M. *J. Chem. Phys.* **1999**, *110*, 2250.
(26) Lyakhova, K. S.; Sevink, G. J. A.; Zvelindovsky, A. V.; Horvat, A.; Magerle, R. *J. Chem. Phys.* **2004**, *120*, 1127.
(27) Horvat, A.; Lyakhova, K. S.; Sevink, G. J. A.; Zvelindovsky, A. V.; Magerle, R. *J. Chem. Phys.* **2004**, *120*, 1117.
(28) Szamel, G.; Mueller, M. *J. Chem. Phys.* **2003**, *118*, 905.
(29) Sevink, G. J. A.; Fraaije, J. G. E. M.; Huinink, H. P. *Macromolecules* **2002**, *35*, 1848.
(30) Huinink, H. P.; Brokken-Zijp, J. C. M.; van Dijka, M. A.; Sevink, G. J. A. *J. Chem. Phys.* **2000**, *112*, 2452.
(31) Wang, Q.; Yan, Q.; Nealey, P. F.; de Pablo, J. J. *J. Chem. Phys.* **2000**, *112*, 450.
(32) Wang, Q.; Nealey, P. F.; de Pablo, J. J. *Macromolecules* **2001**, *34*, 3458.
(33) Knoll, A.; Horvat, A.; Lyakhova, K. S.; Krausch, G.; Sevink, G. J. A.; Zvelindovsky, A. V.; Magerle, R. *Phys. Rev. Lett.* **2002**, *89*, 035501.
(34) Knoll, A.; Magerle, R.; Krausch, G. *J. Chem. Phys.* **2004**, *120*, 1105.
(35) Masten, M. W. *J. Chem. Phys.* **1998**, *108*, 785.
(36) Fukunaga, K.; Hashimoto, T.; Elbs, H.; Krausch, G. *Macromolecules* **2002**, *35*, 4406.
(37) Chen, H. Y.; Fredrickson, G. H. *J. Chem. Phys.* **2002**, *116*, 1137.
(38) Feng, J.; Ruckenstein, E. *Polymer* **2002**, *43*, 5775.
(39) Rehse, N.; Knoll, A.; Magerle, R.; Krausch, G. *Macromolecules* **2003**, *36*, 3261.
(40) Ludwigs, S.; Schmidt, K.; Stafford, C. M.; Amis, E. J.; Fasolka, M. J.; Karim, A.; Magerle, R.; Krausch, G. *Macromolecules* **2005**, *38*, 1850.
(41) Ludwigs, S.; Krausch, G.; Magerle, R.; Zvelindovsky, A. V.; Sevink, G. J. A. *Macromolecules* **2005**, *38*, 1859.
(42) Ludwigs, S.; Boker, A.; Voronov, A.; Rehse, N.; Magerle, R.; Krausch, G. *Nat. Mater.* **2003**, *2*, 744.
(43) Morita, H.; Kawakatsu, T.; Doi, M.; Yamaguchi, D.; Takenaka, M.; Hashimoto, T. *J. Phys. Soc. Jpn.* **2004**, *73*, 1371.
(44) Sides, S. W.; Fredrickson, G. H. *Polymer* **2003**, *44*, 5859.
(45) Yin, Y.; Sun, P.; Chen, T.; Li, B.; Jin, Q.; Ding, D.; Shi, A.-C. *ChemPhysChem* **2004**, *5*, 540.
(46) Sun, P.; Yin, Y.; Li, B.; Chen, T.; Jin, Q.; Ding, D.; Shi, A.-C. *J. Chem. Phys.* **2005**, *122*, 204905.
(47) Suh, K. Y.; Kim, Y. S.; Lee, H. H. *J. Chem. Phys.* **1998**, *108*, 1253.
(48) Yang, Y.; Qiu, F.; Zhang, H.; Yang, Y. *Polymer* **2006**, *47*, 2205.